X-ray absorption study on the origin of the deviation from Vegard's law for U(Al1–xGex)3 solid solution

S. Le Tonquesse, M. Pasturel, Valérie Demange, A. Tayal, P.L. Solari, C. Prestipino

X-ray absorption study on the origin of the deviation from Vegard's law for $U(Al_{1-x}Ge_x)_3$ solid solution

Sylvain Le Tonquesse[a], Mathieu Pasturel[a], Valerie Demange[a], Akhil Tayal[b], Pier Lorenzo Solari[b], Carmelo Prestipino[a,*]

[a] *Univ Rennes, CNRS, ISCR-UMR6226, F-35000, Rennes, France*
[b] *Synchrotron SOLEIL, L'Orme des Merisiers, BP 48, St Aubin, 91192 Gif sur Yvette, France*

Abstract

The cell parameter evolution along the cubic $U(Al_{1-x}Ge_x)_3$ solid solution shows a significant deviation from Vegard's law. The origin of such deviation has been investigated by X-ray powder and electron diffractions, EXAFS and HERFD XANES at the U L_3 and Ge K edges and specific heat measurements. The results of such investigations show that, from the structural point of view, $U(Al_{1-x}Ge_x)_3$ does not present any local or long range ordering and the deviation from Vegard's law is caused by valence instability of U with an actual decrease of the U-Ge bond length with increasing Al-content and cell parameter.

1. Introduction

Similarly to silicon, germanium added to the nuclear material UAl_3 was shown to efficiently block the formation of the undesired UAl_4 during the fabrication process or under irradiation by the reaction of the former with the aluminium matrix in fuel plates or irradiation targets [1]. Moreover, it also has a protective role against the formation of the detrimental ternaries UMo_2Al_{20} and $U_6Mo_4Al_{43}$ in γ-U(Mo)/Al(Ge) diffusion couples simulating prospective fuel plates based on these components [2]. A deep knowledge of the local and long range order of the $U(Al,Ge)_3$ solid solution is thus required to simulate as

*Corresponding author
Email address: carmelo.prestipino@univ-rennes1.fr (Carmelo Prestipino)

precisely as possible the reactivity and irradiation behavior of this fuel. But opposite to the case of $U(Al,Si)_3$ for which numerous data are available in literature [3, 4, 5], scarce reports are available for the $U(Al,Ge)_3$ solid solution [6, 7].

The binary intermetallic compounds UAl_3 and UGe_3 crystallize in the $CuAu_3$ structure-type (*space-group* $Pm\bar{3}m$) where U is located at the *1c* and Al or Ge at the *3a* Wyckoff positions as shown in Fig. 1 (a). Because they crystallize in the same structure-type with relatively close lattice parameters and similar covalent radii [1], (r_{Al} = 1.21 Åand r_{Ge} = 1.20 Å [10]), the existence of a total solid-solution as reported by Tyunis *et al.* [6] and later on by Moussa *et al.* [7] is not surprising. Indeed, similar pseudo-binary systems USn_3-UGa_3, USn_3-UAl_3 [11] and UAl_2-UCo_2 [12] are solid solutions with a complete miscibility and present a conventional evolution of lattice parameters.

For solid solutions, lattice parameters are expected to vary linearly with the composition between the extremities, in accordance with the empirical Vegard's law [13]. The observance of such law agrees with the additivity of covalent radii, as earlier suggested by Pauling and Huggins [14], implying that atomic volumes remain constant independently of the extent of the mixing. However this assumption has been experimentally proven only much later with the development of local range techniques such as EXAFS, because more common Bragg diffraction techniques are based on the coherent scattering generated by long range order, *i.e.* the information obtained are averaged along many unit cells. For instance, in the seminal work of Mikkelsen and Boyce [15], for the first time a solid solution obeying to the Vegard's law, namely zinc-blende $In_xGa_{1-x}As$ (S.G. $F\bar{4}3m$), has been investigated as a function of the composition by EXAFS spectroscopy and diffraction. Bond distances derived from diffraction go from 2.45 Å for GaAs to 2.62 Å for InAs. However, EXAFS detects that lattice

[1] Metallic radii more commonly used in the intermetallics community are also similar, although the actual metallic radius of Ge is less clearly defined (r_{Al}^{metal} = 1.432 Å and r_{Ge}^{metal} = 1.378 Å for Teatum [8] and r_{Ge}^{metal} = 1.43 Å for Batsanov [9]

induced strain affects linearly the bond only up to -2% and +1%, for As-In and As-Ga bonds and consequently two almost constant but clearly different distances are present for all solid solution compositions.

However, although the similitude with the other U pseudo-binary system, both Tyunis *et al.* and Moussa *et al.* [6, 7] reported that the lattice parameter of the $U(Al_{1-x}Ge_x)_3$ solid-solution deviates negatively from linearity and thus violate the Vegard's law. A valence instability of uranium or relative size effects of the *p*-element were evoked, respectively, to explain this observation.

In the present study, a local structure examination of $U(Al_{1-x}Ge_x)_3$ intermetallics with x=0, 0.25, 0.5, 0.75 and 1 using EXAFS and XANES measurements at U L_3 and Ge K-edges has been performed to better understand the structural origin of such deviation and improve the comprehension of chemical bonding in this potential nuclear material.

2. Experimental

Polycrystalline ingots with nominal compositions $U(Al_{1-x}Ge_x)_3$, with x = 0, 0.25, 0.5, 0.75 and 1, were prepared by arc melting stoichiometric amounts of elemental components (all purities $\geq$ 99.5 %). The sample were turned upside down and remelted twice to ensure homogenisation. A subsequent annealing was performed at 973 K for two weeks after enclosing the samples in evacuated silica tubes. Resulting samples have been investigated by X-ray diffraction (XRD) using a Bruker D8 Advance diffractometer ($\theta - 2\theta$ Bragg-Brentano geometry, monochromatized Cu Kα_1, λ = 1.5406 Å) on powders obtained by manually grinding the ingots in an agate mortar. XRD data were modelled with the help of the FullProf code [16]. Scanning electron microscopy was performed using a JEOL JSM 7100 F microscope while electron diffraction and elemental analysis (Energy dispersive spectroscopy,EDS) were performed by transmission electron microscopy on a JEOL 2100 LaB_6 instrument operating at 200kV. To select the smallest particles, powders were suspended in ethanol before deposition on copper grids. Then the grids were kept for a few minutes in air to let the solvent

evaporate.

For X-ray absorption spectroscopy, the $U(Al_{1-x}Ge_x)_3$ powders ($\approx$ 10 mg) were diluted with cellulose in order to achieve a maximum absorbance of ≈ 2, pressed into pellets and then doubled confined in Kapton tape and polyethylene foil. The measurements were carried out on MARS beamline at SOLEIL synchrotron (Saint-Aubin, France) [17]. The X-ray beam energy for measurement at the U L3-edge was selected and scanned using a sagittal focusing Si(220) crystals monochromator and harmonic rejection has been performed by the use of a couple of Pt coated mirrors with an angle of 3.1 mrad. For the measurement at the Ge K-edge, sagittal focusing Si(111) crystals monochromator and Pt mirrors angle of 2.2 mrad were used instead. Extended X-ray Absorption Fine Structure (EXAFS) data have been collected at Ge K edge (11403 eV) and at U L_3 edge (17166 eV) in transmission mode using specific intensity monitors with silicon diodes. Energy calibration has been monitored by measuring simultaneously the absorption of reference sample with residual photons (Y and Ge foils for U L_3 and Ge K edge, respectively). High Energy Resolution Fluorescence Detection (HERFD) X-ray absorption has been also collected on Ge K edge and at U L_3 edge using a spectrometer equipped with a Si(660) or Ge(777) secondary monochomator crystal selecting Ge K-L_3 (9886 eV) and U L_3-M_5 (13615 eV) signals, respectively. For every compositions $U(Al_{1-x}Ge_x)_3$ (x= 0, 0.25, 0.5, 0.75 and 1) fine structures μ(E) after the U L_3 and Ge K edges were measured and converted into χ(R) by Fourier transform using 1, 2 and 3 k-weight and Hanning window with dk = 1. The k-range used for the Fourier transform where 3.5 - 15 $Å^{-1}$ both for the Ge K and U L_3 edges. The fitting procedure was realized simultaneously on the χ(R) of both edges over a range of 1.6 - 3.6 Å for Ge K and 1.6 - 4 Å for U L_3. The coordination spheres around U and Ge as determined from XRD was used to calculate phase and amplitudes employed as initial model for fitting procedure. Reduction and modelling of the data were realized using the IFEFFIT code as implemented in the Athena and Artemis softwares [18]. Finally XANES simulation has been performed using FEFF8.4 code in the muffin-tin real space : full multiple scattering approach. Self-consistent poten-

tial calculations were performed using Hedin-Lundqvist self-energy in a cluster containing around 100 atoms

3. Results

Samples of composition $U(Al_{1-x}Ge_x)_3$ with x=0, 0.25, 0.5, 0.75 and 1 were synthesized and analyzed by powder diffraction (PD). The patterns of all the compositions are indexed with the cubic $CuAu_3$ structure-type ($Pm\bar{3}m$) and only a small amount of UC impurity ($Fm\bar{3}m$) could be detected on the pattern of UAl_3 (Figure 1b). Le Bail refinements of the UAl_3 and UGe_3 patterns converges to lattice parameters of 4.2676(1) Å and 4.2078(2) Å, respectively, in good agreement with literature data [19, 20]. By assuming the solid-solution to follow the Vegard's law, compounds with intermediate composition are expected to have a lattice parameter following the linear relation:

$$a = -0.0199 \cdot x + 4.2676 \text{ Å}. \quad (1)$$

However, experimental lattice parameters found for x= 0.25, 0.5 and 0.75 were 4.2511(2), 4.2271(1) and 4.2132(2) Å, respectively, which indeed correspond to a negative deviation from (1) reaching a maximum of ≈ -0.007 Å in the case of $UAl_{0.75}Ge_{2.25}$.

Deviation from the Vegard's law is not uncommon and were reported for many classes of materials such as oxides, ionic salts or intermetallic. It can originate either from structural effects due to not totally random site occupancies and distortions, such as long range ordering or clustering [21] or from an actual variation of involved bond distances, implying a change in the electron configuration of the material.

Long range ordering phenomena can be detected by diffraction experiments, if their coherence length is sufficient to generate superstructure peaks. For example, in the closely related UAl_3-USi_3 system, crystallizing in the same $CuAu_3$ structure-type ($Pm\bar{3}m$), Meshi *et al.* observed the appearance of satellite

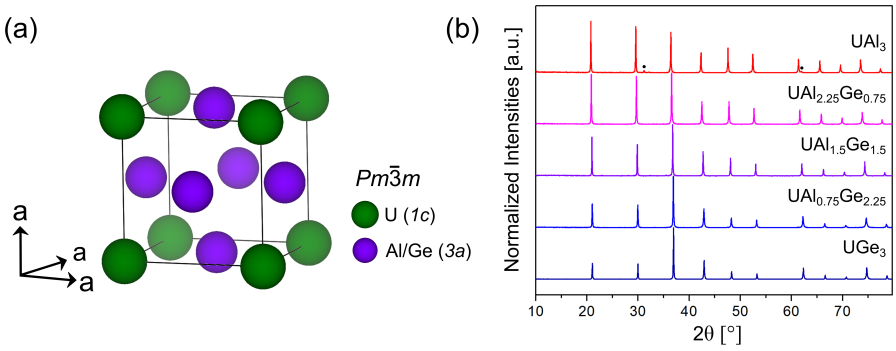

Figure 1: (Color online) (a) Structure of UAl_3 and UGe_3 crystallizing in the $AuCu_3$ structure-type ($Pm\bar{3}m$); (b) powder XRD patterns of the $U(Al_{1-x}Ge_x)_3$ samples with x=0, 0.25, 0.5, 0.75 and 1. The reflections marked with black dots (·) on the UAl_3 pattern correspond to the UC impurity

reflections on the XRD patterns which are explained by the ordering of Al and Si on the *3c* site leading to the formation of a tetragonal superstructure ($I4/mmm$) with lattice parameters $a_t \approx 2a_0$ and $c_t \approx 4a_0$. [4] In our case, no satellite reflections could be detected in any of PXRD patterns, however in order to exclude any ordering at lower range, electron diffraction, which is more sensitive to fine diffraction features, was realized on several grains of powders of compositions $UAl_{1.5}Ge_{1.5}$ and $UAl_{0.75}Ge_{2.25}$ which show the most severe deviation from the Vegard's law.

The electron diffraction patterns recorded along the [001], [011] and [111] zone axis (Figure 2) could be fully indexed with the $CuAu_3$ structure-type ($Pm\bar{3}m$) with similar lattice parameters to those determined from PXRD which confirmed the absence of satellite reflections and superstructure. Moreover all the patterns are composed of very sharp diffraction spots consistent with well crystallized matter and without any type of diffuse scattering which usually appear in case of short range ordering or clustering of atoms. Based on these observations, the $U(Al_{1-x}Ge_x)_3$ compounds seem to be true alloys where the *3c* site is randomly occupied by Al and Ge atoms. At the light of such findings , the origin of lattice parameters deviation form the Vegard's law should not

relate to structural arrangement.

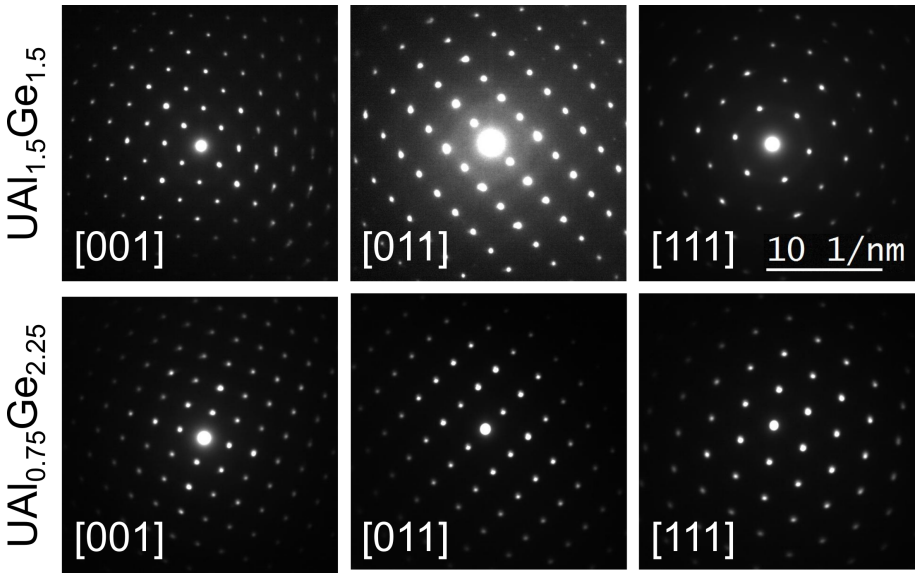

Figure 2: (Color online) Electron diffraction patterns of $UAl_{1.5}Ge_{1.5}$ (top) and $UAl_{0.75}Ge_{2.25}$ (bottom) along the [100] (right), [110] (middle) and [111] (left) zone axis confirming the absence of satellite reflections.

Thus, the non-linear lattice evolution is probably due to electronic effects changing the local structures on the mixed Al/Ge site and preventing the chemical bonds to behave as expected from conventional solid-solution. Examples of such case can be found in $Ce_{1-x}M_xO_2$ (M = Sn and Ti, $0 \geq x \geq 0.5$) where the difference in electronegativities between Ce and Sn provokes a splitting of M-O distances in the first coordination sphere which affects the average distances accessible by diffraction experiments [22]. In order to study atom the local structures and valence states selectively for U and Ge, EXAFS and HERFD X-ray spectroscopy have been performed.

In Fig. 3 the experimental EXAFS signals are shown. Although at a first view the signals seem relatively simple , they are the results of a complex superimposition of several contributes as more visible for sample $UAl_{2.25}Ge_{0.75}$. The local structure of U from crystal data is formed by 12 Al/Ge forming a regular cuboctahedron and 6 more distant U forming a regular octahedra (Fig. 3, right

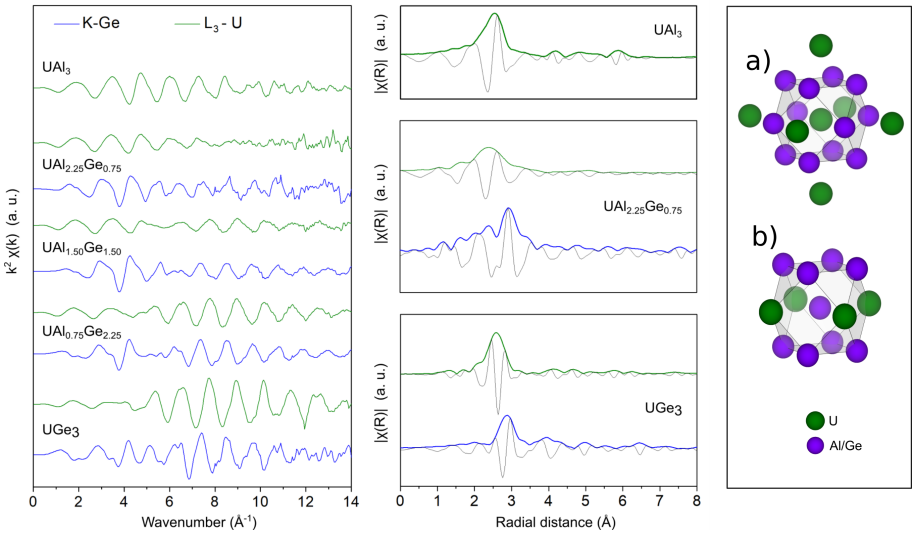

Figure 3: (Color Online) Left and central parts: experimental EXAFS data for $U(Al_{1-x}Ge_x)_3$ solid solution at U L_3 (green curves) and Ge K (blue curves) edges. $\chi(k)k^2$ and imaginary part and magnitude Fourier transform of few selected compositions. Right side: Coordination spheres around U and Ge used as initial model for EXAFS refinements. (a) U-atom coordinated with 12 Al/Ge forming a regular cuboctahedron and 6 more distant U forming a regular octahedra (b) Ge-atom coordinated with 12 Al/Ge forming a regular cuboctahedron

side, part a). As a consequence the apparent single shell signal is generated by the interference pattern of three contributions, two from Al and Ge in the first coordination shell and the third from U in second coordination shell. In the case of Ge, local structure consists of a first coordination shell constituted by a regular cuboctahedron containing 4 U and 8 Al/Ge atoms (Fig. 3, right side, part b), and a second shell formed by a regular octahedra of 6 Ge. However, in the EXAFS signal the second shell contribution is sufficiently separated from the first shell one, consequently, the fitting could be realized considering only the three contributions from the first shell.

In order to evaluate with the maximum precision the near-neighbor (NN) distances around U and Ge, EXAFS signal has been refined simultaneously for the two edges for every compositions taking in account the contribution of the atoms present in the two clusters in fig. 3. All the NN distances U-Al, U-Ge,

Ge-Ge and Ge-Al were initially set equal with value derived from $d = a\sqrt{2}/2$ where a is the lattice parameter obtained from powder diffraction. For U-U contribution, the U-U distances were constrained to the value of a and only the mean square relative displacements (σ^2) were allowed to vary. For the other contributions, the degenerates (N) of Al and Ge were constrained according to the stoichiometry, *i.e.* using a binomial distribution. The refined structural parameters were the NN distances along with their σ^2. Fig. 4 shows the quality of the fits within the R range corresponding to the first coordination spheres (1.0 - 3.75 Å) while Table 1 summarizes the values of the fitted parameters obtained after the refinements. It is worth of noticing, that although the relatively high number of parameters for the fit of a single signal, the correlation between parameters remain rather limited due to the fact that both edges are fitted simultaneously implying that structural parameters remain the same for both signals.

Table 1: Summary of the parameters obtained by combined least square refinements of χ(R) measured at the U L_3 and Ge K egdes for the $U(Al_{1-x}Ge_x)_3$ samples with x=0, 0.25, 0.5, 0.75 and 1. S_0^2, ΔE_0, N and σ^2 correspond to the passive electron reduction function, shift in the edge energy, degeneracy and mean square relative displacements, respectively. Constrained parameters are marked with *.

		UAl_3	$UAl_{2.25}Ge_{0.75}$	$UAl_{1.5}Ge_{1.5}$	$UAl_{0.75}Ge_{2.25}$	UGe_3
U-L_3	S_0^2	0.77(3)	0.75(1)	0.75(5)	0.75(2)	0.82(5)
	ΔE_0 (eV)	5.6(3)	5(1)	6.2(7)	4(1)	5.2(7)
	N Al/Ge	12/0*	9/3*	6/6*	3/9*	0/12*
Ge-K	S_0^2	/	1.0(3)	0.81(9)	0.9(1)	0.79(8)
	ΔE_0 (eV)	/	2.99(1)	3(1)	1.9(6)	2.3(7)
	N U/Al/Ge	/	4/6/2*	4/4/4*	4/2/6*	4/0/8*
bond distances	*U-Ge* (Å)	/	2.945(6)	2.946(3)	2.951(1)	2.970(1)
	σ^2 (Å^2)	/	0.007(2)	0.006(1)	0.0067(2)	0.0057(4)
	U-Al (Å)	3.022(1)	3.017(5)	3.011(3)	2.984(7)	/
	σ^2 (Å^2)	0.0069(6)	0.008(1)	0.007(1)	0.011(4)	/
	U-U (Å)	4.2676*	4.2511*	4.2271*	4.2132*	4.2078*
	σ^2 (Å^2)	0.007(1)	0.04(3)	0.027(8)	0.018(5)	0.009(2)
Agreement factors	χ^2	92.2	188.7	46.8	66.2	110.1
	R-factor	0.021	0.039	0.023	0.007	0.016

The χ(R) of UAl_3 and UGe_3, shown in Figure 4 (a) and (e), could be fitted using a single NN distance of 3.022 Å for U-Al and 2.975 Å for U-Ge in good agreement with XRD distances (3.017 Å and 2.975 Å , respectively) proving the adequacy of the approximation of considering the calculation of phase and amplitude for U L_3 sufficiently precise to be directly compared with powder diffraction. It is worth to notice that for the alloys, no satisfactory fit could be obtained constraining U-Al and U-Ge to the same bond length. Appropriate fits (Fig. 4 (b)-(d)), could be achieved only using two different bond lengths as expected from the previous solid solution works on local structure.

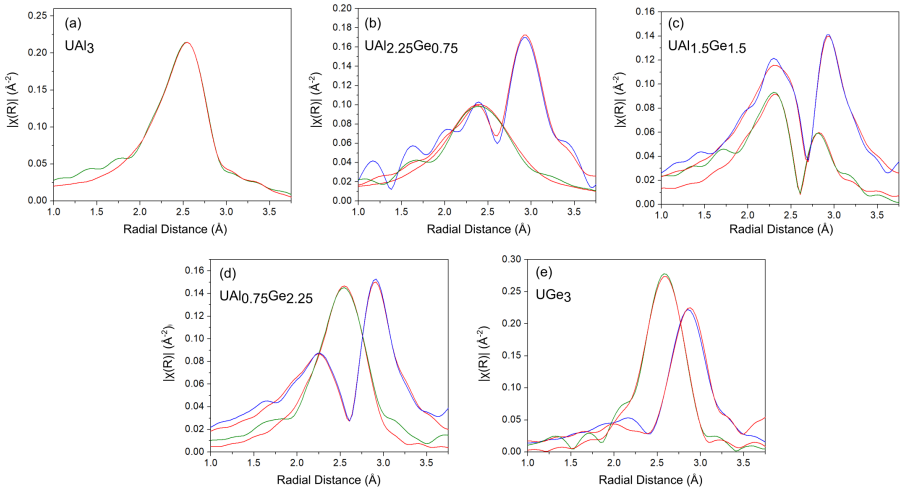

Figure 4: (Color Online) Fits of the χ(R) for all the compositions studied in the 1.0 to 3.75 Å range corresponding to the first coordination sphere of U- and Ge-atoms in the $U(Al_{1-x}Ge_x)_3$ solid solution. χ(R) of the Ge K and U L_3 edges are plotted in blue and green, respectively. Results of the fits are plotted in red.

Fig. 5 shows the evolution of the U-Ge and U-Al distances as a function of the concentration x of Ge in $U(Al_{1-x}Ge_x)_3$ along with the average U-(Al/Ge) distance determined by XRD and by a weighted average of the distances obtained by EXAFS analysis, calculated with:

$$\text{U-Al/Ge} = \text{U-Ge} \cdot x + \text{U-Al} \cdot (1 - x) \tag{2}$$

With increasing the Ge-content in UAl_3, the U-Al distance was found to shorten from 3.022(4) Å in UAl_3 to 2.98(2) Å in $UAl_{0.75}Ge_{2.25}$. As mentioned before, this is the typical behavior of conventional solid solutions where only a light shortening of distance, due the increasing crystal strain, is expected. On the other hand, the U-Ge distance, in discrepancy with crystallography prediction where the distance is supposed to increase due to the bigger cell parameter of UAl_3, decreases with increasing Al concentration from 2.969Å in UGe_3 to 2.941 Å in $UAl_{2.25}Ge_{0.75}$ ($\approx$ -1 % shortening).

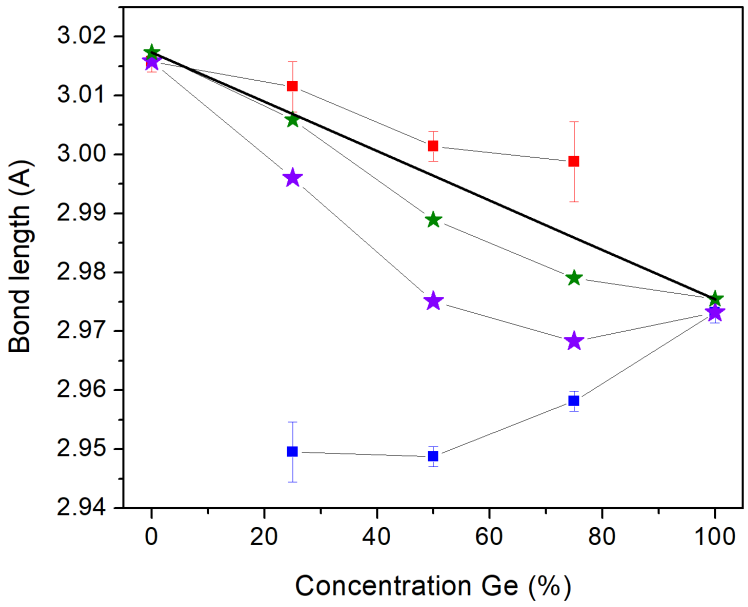

Figure 5: (Color Online) Evolution of the U-Al (blue squares), U-Ge (red squares) and average U-Al/Ge distances (purple stars) obtained from EXAFS as a function of the Ge concentration x in $U(Al_{1-x}Ge_x)_3$ intermetallics. Distances determined from XRD (green stars) and the linear relation expected from the Vegard's law (black line) are shown for comparison of the evolution obtained by the two methods.

As a consequence the average U-Al/Ge distance, strongly deviates from the linear evolution expected from the Vegard law. Remarkably , the trend of the

deviation calculated from EXAFS data is in good agreement with the deviation measured by XRD since both are negative and with the maximum deviation for the $UAl_{1.5}Ge_{1.5}$ and $UAl_{0.75}Ge_{2.25}$ compositions. However, the extent of such deviation is systematically higher for EXAFS data in respect to XRD, suggesting the possible existence of medium range distortion that tends to accommodate the bond distance differences. In this context the deviation from Vegard's law is directly caused by the abnormal shortening of the U-Ge distance with increasing Al-content.

In order to investigate the origin of such Ge-U bond behavior, the evolution of XANES spectra as a function by of the composition was measured by high energy resolution fluorescence detection (HERFD) on the two U L_3 and Ge K edges. HERFD is an acquisition mode for X-ray absorption in which the fluorescence signal is recorded with crystal analyzer with an energy resolution higher than the core hole [23]. Such setup has the major effect to keep constant the exchange energy during the photon in photon out process, with the consequence of replacing in the spectral broadening the contribution of the photon excited core level with the one related to the fluorescence emission. In the present case, it enabled to replace the intrinsic resolution for U spectra from 8.16 eV to 3.94 eV and for Ge from 2.36 eV to 0.76 eV.

The HERFD spectra for the studied compositions for both U L_3 edge and Ge K edge are shown in Fig. 6. The U L_3 edge is dominated by the dipole allowed transition $2p \rightarrow 6d$ commonly called white line at around 17175 eV. The XANES spectroscopy of Uranium based intermetallics, has been widely investigated by several groups [24, 25, 26, 27], determining a good correlation between the position of the white line peak with f levels population. In this context the progressive blue shift of the white line and edge position as the Al concentration increases should be interpreted as a limited depopulation (oxidation) of U *5f* levels of around 0.2 e^- taking in account a shift around 2 eV[24]. The observation is in agreement with the work of Tyunis *et al.* [6] that have investigated the same solid solution by high resolution analysis of fluorescence emission, determining the number of *5f* electrons of uranium to 2.54 for UGe_3

and 2.26 for UAl_3 (*i.e.* depopulation of 0.28 e^-).

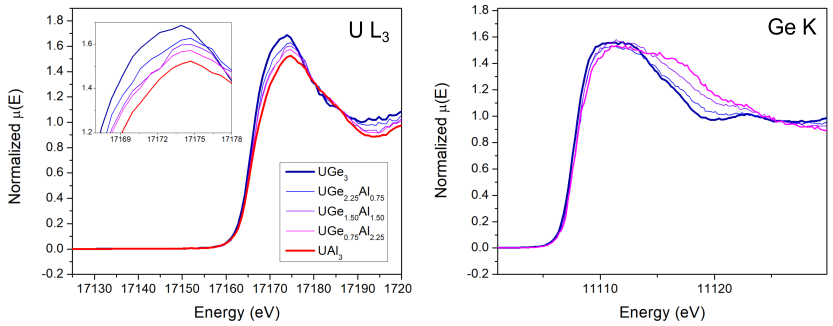

Figure 6: (Color Online) HERFD of the U L_3 XANES for $U(Al_{1-x}Ge_x)_3$ with x=0, 0.25, 0.5, 0.75 and 1. The inset is a close up view showing the continuous evolution in energy of the peak edge toward higher energies with increasing Al content.

The Ge K edge is dominated by the $1s \rightarrow 4p$ transition. In such case the spectral change is more limited than U, the edge is almost unaffected and the increase of Al concentration generates a minor decrease of the white line peak and a clear increase of the shoulder at 11118 eV. XANES simulations using the structure of UGe_3 and an UGe_2Al model using experimental interpolated cell parameters and a $P4/mmm$ superstructure are able to reproduce the main features of the spectra evolution (see SI fig. 1, 2 and 3). Using such approximation is possible to compare the spectra characteristics with the density of states obtained during the same calculation. It emerges that at Ge K edge, the two peaks at 11110 and 11118 eV that are mainly due to Ge levels with p character, fall in the same energy range than two peaks of U dos with d character suggesting that Al in the solid solution actively affect the hybridization of U d levels with the Ge p levels.

The depopulation of the U-$5f$ orbitals with increasing aluminum content is supported by specific heat measurements (fig. 7). Despite some noise at the lowest temperatures in the signal of UAl_3 due to the non-congruent melting of this phase [14, 7] inducing the appeareance of porosity and cracks after annealing, the specific heat follows up to about 10 K the expected law for a regular

metal:

$$\frac{C_p}{T} = \gamma + \beta T^2 \quad (3)$$

where γ is the Sommerfeld coefficient and β the Debye component of the specific heat.

The specific heat of UAl_3 agrees with previous reports, showing an almost flat variation of $C_p/T = f(T^2)$ below 100 K^2 ($\beta = 0.118$ mJ mol^{-1} K^{-4}) and a Sommerfeld coefficient of 43 mJ mol^{-1} K^{-2} (41, 41.6, 43.2 and 47 mJ mol^{-1} K^{-2} for Scheidt [11], van Maaren [28], Cornelius [29] and Aoki [30] *et al.*, respectively). The values obtained for UGe_3 ($\beta = 0.49$ mJ mol^{-1} K^{-4}, $\gamma = 20.2$ mJ mol^{-1} K^{-2}) are also in line with literature data (β =0.455 mJ mol^{-1} K^{-4} [28] - γ = 20.4 [28, 31], 20.5 mJ mol^{-1} K^{-2} [11]). With the exception of $UAl_{2.25}Ge_{0.75}$, β increases regularly with the Ge-content, in agreement with the heavier molar mass of this element. γ follows an opposite increase with the Al-content along the solid solution. Such an increase highlight an enhanced contribution of the electrons to the specific heat which is usually attributed to a higher delocalization of the U-*5f* electrons, in agreement with the spectroscopic observations.

The anomalous behavior of $UAl_{2.25}Ge_{0.75}$, confirmed by C_p measurements on several pieces with this composition, remains unexplained yet.

4. Conclusion

In the present work the origin of the deviation from the Vegard's law for $U(Al_{1-x}Ge_x)_3$ has been investigated experimentally by long and local range order techniques. The deviation has been proven to be based on actual bond length variation while the possible long range ordering phenomena as UAl_3-USi_3 has been excluded by the absence of superstructures or diffuse scattering in electron diffraction. Indeed the deviation is mainly related to a decrease of U-Ge bond length induced by the increase of Al concentration in the solid solution.

HERFD XANES and specific heat measurements show that such unexpected decrease of bond length is related to the depopulation of the U *5f* levels (around

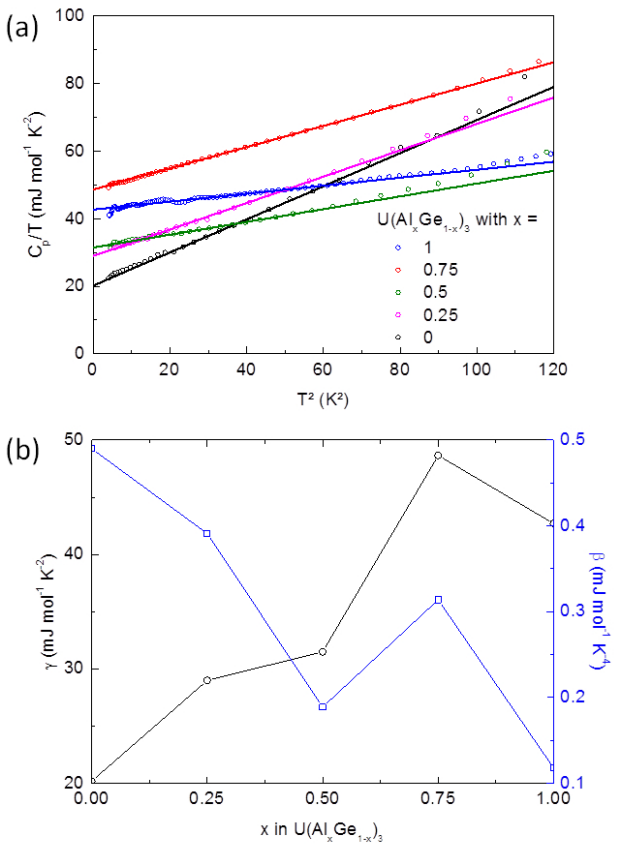

Figure 7: (Color Online) (a) Thermal dependence of the specific heat of UAl_xGe_{3-x} for x = 0, 0.25, 0.5, 0.75 and 1 (symbols) and linear fit according to eq. (3); (b) Variation of the γ (left) and β (right) parameters with the chemical composition, extracted from these fits (the solid lines are guides for the eyes). The standard deviations on the values are below the thickness of the symbols.

0.2 e^-) suggesting that the deviation from Vegard's law is caused by valence instability in agreement with the work by Tyunis *et al.*[6].

Finally, such valence instability, in accordance with XANES simulations, seem to be related to the hybridization of Ge *4p* levels with U *6d* levels.

Acknowledgements

Vincent Dorcet is acknowledged for TEM experiments performed on THEMIS platform part of the ScanMAT unit (UMS 2001, University of Rennes 1), which received a financial support from the European Union (CPER-FEDER 2007–2014).

References

[1] W. C. Thurber, R. Beaver, Development of silicon-modified 48 wt.% u-al alloys for aluminum plate-type fuel elements, Tech. rep., Oak Ridge National Lab., Tenn. (1959). doi:10.2172/4260852.

[2] E. Perez, D. Keiser, Y. Sohn, Phase development in a u–7wt. % mo vs. al–7wt. % ge diffusion couple, Journal of Nuclear Materials 441 (1) (2013) 159 – 167. doi:https://doi.org/10.1016/j.jnucmat.2013.05.069.

[3] D. Rabin, R. Z. Shneck, G. Rafailov, I. Dahan, L. Meshi, E. Brosh, Thermodynamic modeling of al–u–x (x= si, zr), Journal of Nuclear Materials 464 (2015) 170–184.

[4] G. Rafailov, I. Dahana, L. Meshi, Acta Cryst. B70 (2014) 580.

[5] H. J. Ryu, Y. S. Kim, G. L. Hofman, J. M. Park, C. K. Kim, Heats of formation of (u, mo) al3 and u (al, si) 3, Journal of nuclear materials 358 (1) (2006) 52–56.

[6] A. V. Tyunis, V. A. Shaburov, Y. P. Smirnov, A. E. Sovestnov, Valence instability of uranium in U(Al1-x Gex)3, Physics of the Solid State 39 (9) (1997) 1337–1340. doi:10.1134/1.1130075.

[7] C. Moussa, Z. ElSayah, G. Chajewski, A. Berche, V. Dorcet, A. Pikul, M. Pasturel, L. Joanny, B. Stepnik, O. Tougait, J. Solid State Chem. 243 (2016) 168.

[8] E. T. Teatum, Compilation of calculated data useful in predicting metallurgical behavior of the elements in binary alloy systems, Los Alamos

Scientific Laboratory of the University of California, 1968, citation Key: teatumCompilationCalculatedData1968.

[9] S. S. Batsanov, Metallic radii of nonmetals, Russian Chemical Bulletin 43 (2) (1994) 199–201. doi:10.1007/BF00695809.

[10] B. Cordero, V. Gómez, A. E. Platero-Prats, M. Revés, J. Echeverría, E. Cremades, F. Barragán, S. Alvarez, Covalent radii revisited, Dalton Trans. (2008) 2832–2838doi:10.1039/B801115J.

[11] E.-W. Scheidt, G. Fraunberger, J. Rieger, A. Mielke, W. Kim, G. Stewart, J Alloys Compd. 218 (1995) 5.

[12] E. Burzo, P. Lucaci, Solid State Commun. 56 (1985) 537.

[13] L. Vegard, Z. Phys. 5 (1921) 17.

[14] L. Pauling, M. L. Huggins, Covalent Radii of Atoms and Interatomic Distances in Crystals containing Electron-Pair Bonds, Zeitschrift für Kristallographie - Crystalline Materials 87 (1-6) (1934) 205. doi:10.1524/zkri.1934.87.1.205.

[15] J. C. Mikkelsen, J. B. Boyce, Phys. Rev. Lett. 49 (1982) 1412.

[16] J. Rodriguez-Carvajal, Physica B 192 (1993) 55.

[17] B. Sitaud, P. L. Solari, S. Schlutig, I. Llorens, H. Hermange, J. Nucl. Mater. 425 (2012) 238.

[18] B. Ravel, M. Newville, J. Synchrotron Rad. 12 (2005) 537.

[19] H. N. O. Tougait, Intermetallics 12 (2004) 219.

[20] J. F. Jr., G. H. Lander, J. Brown, A. Delapalme, Acta Cryst. 37 (1981) 558.

[21] M. Castellanos, A. R. West, J. Chem. Soc. Faraday Trans. 76 (0) (1980) 2159–2169. doi:10.1039/F19807602159.

[22] T. Baidya, P. Bera, O. Krocher, O. Safonova, P. M. Abdala, B. Gerke, R. Pottgen, K. R. Priolkarg, T. K. Mandalh, Phys. Chem. Chem. Phys. 18 (2016) 13974.

[23] J. A. v. Bokhoven, C. Lamberti (Eds.), X-ray absorption and X-ray emission spectroscopy: theory and applications, John Wiley & Sons, Inc, Chichester, West Sussex, 2015.

[24] C. H. Booth, Y. Jiang, D. L. Wang, J. N. Mitchell, P. H. Tobash, E. D. Bauer, M. A. Wall, P. G. Allen, D. Sokaras, D. Nordlund, T.-C. Weng, M. A. Torrez, J. L. Sarrao, Multiconfigurational nature of 5f orbitals in uranium and plutonium intermetallics, Proceedings of the National Academy of Sciences 109 (26) (2012) 10205–10209. doi:10.1073/pnas.1200725109.

[25] C. H. Booth, S. A. Medling, Y. Jiang, E. D. Bauer, P. H. Tobash, J. N. Mitchell, D. K. Veirs, M. A. Wall, P. G. Allen, J. J. Kas, D. Sokaras, D. Nordlund, T. C. Weng, Delocalization and occupancy effects of 5f orbitals in plutonium intermetallics using L3-edge resonant X-ray emission spectroscopy, Journal of Electron Spectroscopy and Related Phenomena 194 (2014) 57–65. doi:10.1016/j.elspec.2014.03.004.

[26] C. H. Booth, S. A. Medling, J. G. Tobin, R. E. Baumbach, E. D. Bauer, D. Sokaras, D. Nordlund, T.-C. Weng, Probing $5f$-state configurations in ${\mathrm{URu}}_{2}{\mathrm{Si}}_{2}$ with U ${L}_{\text{III}}$-edge resonant x-ray emission spectroscopy, Phys. Rev. B 94 (4) (2016) 045121. doi:10.1103/PhysRevB.94.045121.

[27] K. O. Kvashnina, H. C. Walker, N. Magnani, G. H. Lander, R. Caciuffo, Resonant x-ray spectroscopy of uranium intermetallics at the ${M}_{4,5}$ edges of uranium, Phys. Rev. B 95 (24) (2017) 245103. doi:10.1103/PhysRevB.95.245103.

[28] M. Van Maaren, H. Van Daal, K. Buschow, C. Schinkel, High electronic specific heat of some cubic ux3 intermetallic compounds, Solid State Communications 14 (2) (1974) 145–147.

[29] A. Cornelius, A. Arko, J. Sarrao, J. Thompson, M. Hundley, C. Booth, N. Harrison, P. Oppeneer, Electronic properties of u x 3 (x= ga, al, and sn) compounds in high magnetic fields: Transport, specific heat, magnetization, and quantum oscillations, Physical Review B 59 (22) (1999) 14473.

[30] D. Aoki, N. Watanabe, Y. Inada, R. Settai, K. Sugiyama, H. Harima, T. Inoue, K. Kindo, E. Yamamoto, Fermi surface properties of the enhanced pauli paramagnet ual 3, Journal of the Physical Society of Japan 69 (8) (2000) 2609–2614.

[31] A. Pikul, R. Troć, A. Czopnik, H. Noël, Low-temperature specific heat of uranium germanides, Journal of Magnetism and Magnetic Materials 360 (2014) 217–221.

Supplementary

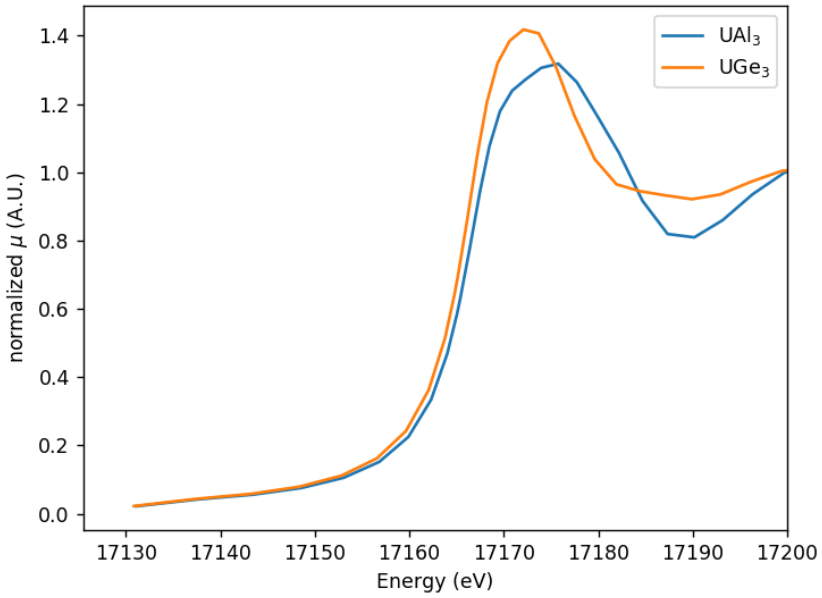

Figure 8: (Color Online) U edge. Simulation of of UGe_3 and UAl_3 curve blue and orange respectively. As for experimental the UAl_3 whiteline is broader and blueshift

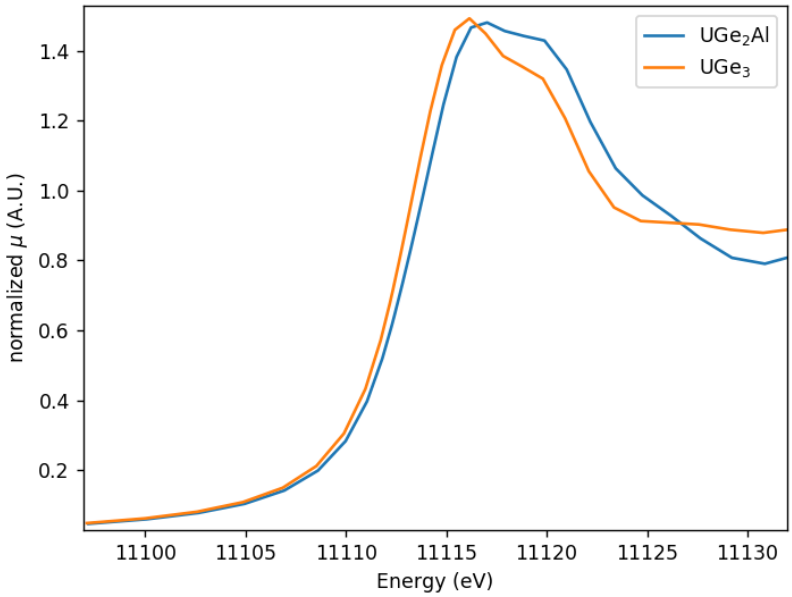

Figure 9: (Color Online) Ge K-edge simulation UGe_2Al and UGe_3 curve blue and orange respectively. Study of the modification of Ge edge as a function of Al concentration. The UGe_2Al cluster has been generating using $P4/mmm$ superstructure

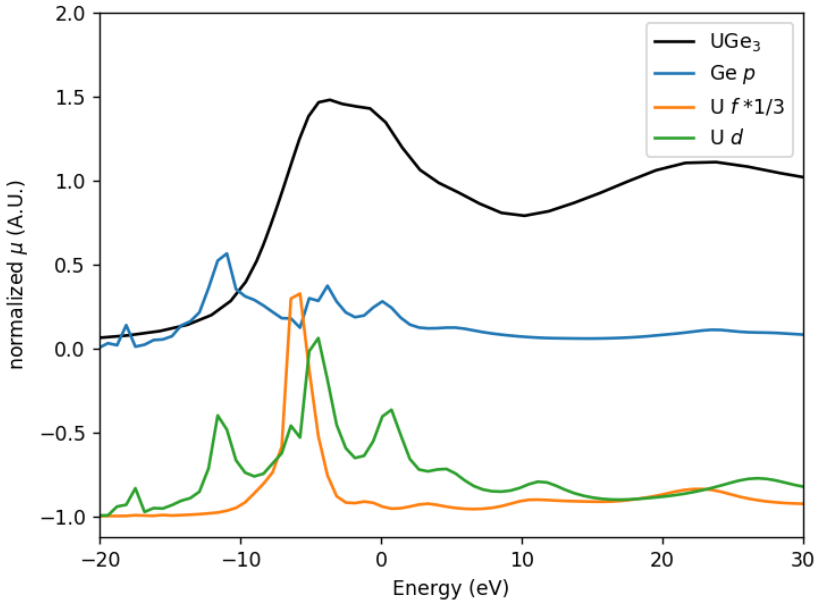

Figure 10: (Color Online) Ge K-edge simulation of UGe_2Al and related symmetry filtered projected density of state for each atoms.

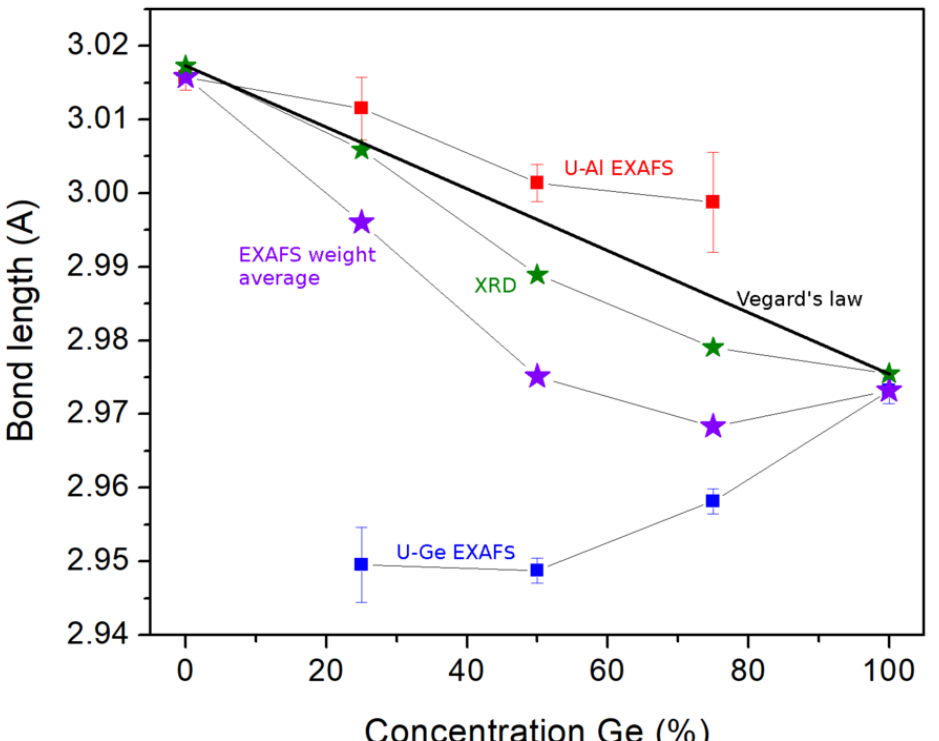
Unusual variation of the U-Ge distance explains
U(Al1−xGex)3 deviation from Vegard's law
Bond length (A)
3.02
3.01
3.00
2.99
2.98
2.97
2.96
2.95
2.94
0
20
40
60
80
100
Concentration Ge (%)
U-Al EXAFS
EXAFS weight
average
XRD
Vegard's law
U-Ge EXAFS